



Laboratory time-resolved X-ray diffractometry for *in situ* studies of crystalline materials under uniaxial compression and vibration

Valentin Akkuratov,^{a,b*} Alexander Blagov,^{a,b} Yan Eliovich,^{a,b} Anton Targonskii,^{a,b} Yuri Pisarevsky,^{a,b} Andrei Protsenko,^{a,b} Vladimir Shishkov^a and Mikhail Kovalchuk^{a,b}

Received 4 March 2021

Accepted 22 November 2021

Edited by D. I. Svergun, European Molecular Biology Laboratory, Hamburg, Germany

Keywords: time-resolved studies; high-resolution X-ray diffraction; mechanics of materials.

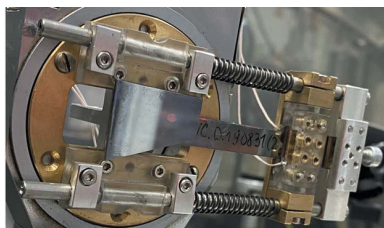
^aFederal Scientific Research Centre 'Crystallography and Photonics', Russian Academy of Sciences, Leninskii prospekt 59, Moscow, 119333, Russian Federation, and ^bNational Research Centre 'Kurchatov Institute', Akademika Kurchatova ploshchad 1, Moscow, 123182, Russian Federation. *Correspondence e-mail: akkuratov.val@gmail.com

A novel laboratory diffractometer for time-resolved high-resolution X-ray diffraction studies of reversible and irreversible processes in crystalline materials under uniaxial compression and vibration is described. Temporal resolution up to milliseconds for double-crystal and up to tens of seconds for triple-crystal diffraction experiments was achieved with a single adaptive bending X-ray optics element. Design solutions and techniques for applying and controlling uniaxial compression and vibration for *in situ* time-resolved studies are described. Results are presented for various static and dynamic load experiments, controlled by a system based on the *TANGO Controls* framework. Rocking curves of paratellurite (TeO₂) under quasi-static compression and lithium fluoride (LiF) under ultrasonic vibration were measured with temporal resolution. Reciprocal-space maps of LiF under static compression and quartz (SiO₂) under ultrasonic vibration were collected.

1. Introduction

X-ray diffraction, which allows high-precision and non-destructive measurements, is one of the most powerful methods for studying crystalline materials. Among various diffraction techniques, double-crystal and triple-crystal high-resolution X-ray diffractometry (HRXRD) is widely used for fast and integral characterization of defect structure (Pietsch *et al.*, 2004; Bowen & Tanner, 1998; Nespolo, 2019). [In this paper, the terms 'structure' and 'lattice' are used as discussed by Nespolo (2019).]

A critical factor limiting the possibilities of X-ray diffraction and scattering for studying fast processes is the speed of tuning X-ray beam parameters (angle, wavelength, intensity). Conventional X-ray diffractometry experiments require the movement and rotation of optical scheme units such as beam-forming and detection equipment or the sample itself. That is usually related to slow, complicated, inertial instrumentation systems, which significantly limit temporal resolution. The use of diffractometers based on these systems limits the possibilities for investigating fast processes, such as the effect of various external influences on the material's structure. The effect of mechanical stress, vibration, temperature gradient, and electric and magnetic fields is the subject of numerous studies. In particular, studying deformation behavior under compression and vibration load allows one to predict the reliability of crystalline microelectronic components, to control properties of semiconductor crystals (Sinno *et al.*, 2000), and to implement straintronics (Bukharaev *et al.*, 2018)



or elastic strain engineering (Li *et al.*, 2014). Typically, in these studies, the characteristics of the samples are measured before and after the external influence. This approach only provides indirect information about the sample during the exposure.

In situ time-resolved X-ray diffraction studies can reveal sample dynamics directly during the exposure process. Instead of mechanical systems, time-resolved studies can be implemented using piezo actuators based on piezoceramics or single crystals. Such actuators and actuator-based systems are commonly used due to their unique characteristics (high speed and wide angular scanning range) as different motors and stages (Morita, 2003; Matsunami *et al.*, 2008), for fast optical beam scanning (Filhol *et al.*, 2005), as beam deflectors (Tsai *et al.*, 2015) or even for time-resolved quick-scanning EXAFS (Richwin *et al.*, 2002).

Piezo actuators based on bending oscillations are expected to find promising applications in X-ray diffractometry for ω or

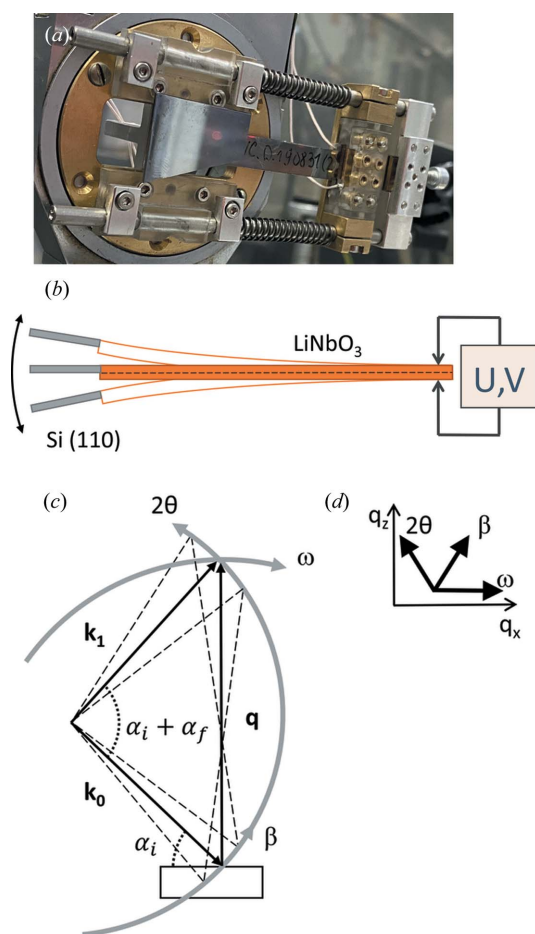


Figure 1

(a) A photograph of the ABXO element. (b) The ABXO consists of an LiNbO₃ bidomain single crystal and Si(110) crystal plate. (c) Directions of scans in reciprocal space in the case of a single ABXO element installed as monochromator in a triple-crystal experiment. Axis β is defined by changing the angle (α_i) between the incident X-ray beam and the sample surface. The angle α_i changes because the ABXO element oscillates, and a 'triangle' of \mathbf{k}_0 , \mathbf{k}_1 , \mathbf{q} vectors slides along the Ewald sphere (\mathbf{k}_0 and \mathbf{k}_1 are the wavevectors of the incident and diffracted beams, and \mathbf{q} is the scattering vector). Scans of reciprocal space are shown with thick gray arrows (ω , 2θ and β). In (d), scan directions in reciprocal space are shown together.

energy scanning and as beam choppers. Unlike piezoceramics, piezoelectric crystals have no hysteresis of mechanical properties. Typically, a piezo crystal bending actuator consists of two identical crystal plates connected by faces. The electric field application causes one plate to expand and another to compress, forcing the entire element to bend (Shur *et al.*, 2015). However, this design makes the piezo actuator unreliable due to the plate connection and unsuitable for accurate diffraction measurements.

An adaptive bending X-ray optics element (ABXO) (Blagov *et al.*, 2016; Eliovich *et al.*, 2018) based on a monolithic bimorph LiNbO₃ piezo actuator is free of this drawback. In these actuators, a structure of two domains with equal thickness and opposite electric polarization vectors is realized in the same piezoelectric single crystal by specialized annealing technology (Nakamura & Shimizu, 1989; Bykov *et al.*, 2014; Malinkovich *et al.*, 2013). The two-domain structure makes the ABXO element a hysteresis-free and precise instrument for time-resolved X-ray diffraction studies. Typically, the ABXO element consists of a piezoelectric actuator and a high-quality crystal attached to its end [Fig. 1(a)]. This high-quality crystal interacts with an X-ray beam. Applying an alternating electric field to the actuator causes bending oscillations [Fig. 1(b)] (Blagov *et al.*, 2016). The bending allows one to control the change in the angular position of the high-quality X-ray optical crystal relative to the incident beam. Parameters of the control electric field determine the ABXO operating mode.

This article describes basic principles and module design for the implementation of time-resolved X-ray diffraction with the ABXO. Also, the experimental results for the behavior of crystalline materials under static and quasi-static uniaxial compression and vibration are presented.

2. Methods

2.1. Double-crystal and triple-crystal diffractometry

The double-crystal X-ray diffraction technique is used for rocking curve measurement. The rocking curve is the intensity distribution of the diffracted X-ray beam on its incidence angle on the sample. Rocking curve analysis, including comparison with theoretical models, makes it possible to determine the degree of perfection of a crystalline structure and its defects (Bowen & Tanner, 1998). There are only two crystals in the optical scheme in double-crystal diffraction measurements: the X-ray monochromator and the sample. The detector registers the intensity of the diffracted X-ray beam after the sample. Typically, the registration of a rocking curve takes several minutes.

Triple-crystal diffraction is used for acquiring reciprocal-space maps (RSMs). These maps contain the intensity distribution in the vicinity of a reciprocal-lattice point (Iida & Kohra, 1979; Fewster, 1997). An analyzer crystal is installed in front of the detector in addition to the double-crystal scheme X-ray optical elements. The principal scheme is presented in Section 3.1. An RSM is a set of line scans (rocking curves) collected at different angular offsets of the analyzer crystal.

The result is the X-ray intensity map, where the coordinates are the angular positions of the analyzer and the sample relative to the incident X-ray beam. An RSM provides more information than a single line scan and is used to aid the interpretation of displacement, broadening or overlapping of diffraction peaks. Reciprocal-space mapping requires hours of measurements.

There are two basic geometries for X-ray double-crystal and triple-crystal diffraction experiments. In the reflection (Bragg) geometry, crystal planes parallel to the sample surface are studied [Section 3.2, Fig. 3(a)]. Usually, in this geometry the X-ray beam can probe only a thin near-surface layer tens of micrometres thick. In the transmission (Laue) geometry, the beam penetrates through the sample [Fig. 3(c)]. This geometry allows one to study crystal planes perpendicular to the sample surface and investigate structure on the beam trajectory inside the crystal volume.

2.2. Adaptive X-ray optics in double-crystal and triple-crystal diffractometry

There are two ways to use a single ABXO element in double-crystal and triple-crystal experiments. Both approaches allow one to measure crystalline samples that can be studied using classical double-crystal and triple-crystal diffractometry without additional preparation.

The ABXO element can be installed as a monochromator or an analyzer. In this case, it is possible to control the angular position of the X-ray beam with the ABXO with negligible changes in the spectrum and spatial displacement. An in-plane spatial displacement of the beam occurs due to the bend of the ABXO element. It depends on the oscillation amplitude of the ABXO element and the distance between it and the next optic element, and does not exceed tens of micrometres. If the ABXO is installed as a monochromator and the X-ray source generates a diverging radiation beam like an X-ray tube (Section 3.1, Fig. 2), the beam is not blocked by the collimation slit (Eliovich *et al.*, 2018).

The ABXO element can be combined with the sample (Kohn *et al.*, 2020). In this case, the sample is attached instead of an Si crystal to the piezo actuator. With this setup, narrow (up to tenths of an arcsecond) rocking curves can be measured, with precise control of the sample position with respect to the beam. However, experimentation with external influences is technically challenging due to the high sensitivity of the piezo actuator. Therefore, this method is used only for studying model processes and is not considered in this article.

A reciprocal-space scan occurs differently depending on the ABXO element position in double-crystal or triple-crystal experiments. In a double-crystal experiment, an ABXO element scan occurs along the ω axis. In a triple-crystal experiment, scanning occurs along the β axis [Fig. 1(c)], different from ω or 2θ (Eliovich *et al.*, 2020). In the case of an ABXO element installed as a monochromator, the β axis is defined by changing the angle (α_i) between the incident X-ray beam and the sample surface. The angle (α_i) changes because of the ABXO element oscillations. In this paper, a combination of ABXO monochromator (β scan) and single stepper

motor (2θ scan) is used for reciprocal-space mapping, and the coordinates of the scattering vector \mathbf{q} can be described by

$$\begin{aligned} k &= 2\pi/\lambda, \\ q_x &= k[\cos(\alpha_f) - \cos(\alpha_i)], \\ q_z &= k[\sin(\alpha_i) + \sin(\alpha_f)], \\ \alpha_i &= \beta, \\ \alpha_f &= \theta_{\text{Bragg}} + \Delta, \end{aligned} \quad (1)$$

where λ is the X-ray wavelength, α_i is the angle of incidence of the X-ray beam on the sample relative to the sample surface, β is the angle determined by the oscillations of the bending monochromator, α_f is the angle of the X-ray beam reflected from the sample relative to the sample surface and Δ is a small angular offset determined by the 2θ scan.

2.3. Adaptive X-ray optics and time-resolved studies

The measurement speed of the ABXO element depends on two fundamental factors. The first factor is the X-ray source brightness. The higher the brightness, the greater is the achievable temporal resolution. The second factor is the oscillation frequency of the piezo crystal. It depends on the operating mode and determines the maximum temporal resolution, which is microseconds for this technique. Experimental results (Marchenkov *et al.*, 2019) indicate that the limit determined by the frequency can be reached only with third- and fourth-generation synchrotron sources and fast detectors. Scintillation detectors or detectors based on avalanche photodiodes can be used (Kishimoto *et al.*, 1998).

Quasi-static operating mode (Kulikov *et al.*, 2019) is provided by a triangular low-frequency (less than 10 Hz) control signal. This mode simplifies data processing since the signal amplitude dependence on time is linear. In this operating mode, angular scans with steps up to 10^{-7}° are ensured. Typically, precision goniometric systems for synchrotron diffractometers have driving step size up to 10^{-4}° (He, 2018). However, in quasi-static mode, the scanned angular range does not exceed hundreds of arcseconds.

Resonant operating mode is provided by applying a sinusoidal electric signal with the ABXO natural frequency. The frequency limits the maximum temporal resolution to microseconds. At a second-generation synchrotron, a rocking curve was recorded with a temporal resolution of 108 μs (Marchenkov *et al.*, 2019). The rocking curve acquisition time achieved in transmission geometry with an X-ray tube was 1.5 s (Eliovich *et al.*, 2018). For an RSM collected with the combination of a single ABXO element (in the position of monochromator or analyzer) and stepper motor, the acquisition time is about 5 min (Eliovich *et al.*, 2020).

The main objectives of the studies at laboratory X-ray sources with a single ABXO element were formulated taking into account achievable temporal resolution.

In situ time-resolved studies with double-crystal diffractometry. The ABXO allows one to measure rocking curves continuously in an angular range up to 1° with temporal resolution from seconds to milliseconds, depending on the

ordering of the sample, the experiment geometry and the brightness of the X-ray source. Such a setup allows one to study processes at a time scale from minutes to days.

In situ fast diagnostics of crystalline materials using triple-crystal diffractometry. Reciprocal-space mapping takes a few (up to 5) minutes and depends on the number of rocking curves and their temporal resolution. For data collection, a combination of a single ABXO element and a step motor is used. Thus, the temporal resolution of the RSM strongly depends on the angular range scanned with a step motor.

In situ time-resolved studies of crystalline materials with triple-crystal diffractometry. For time-resolved studies (up to tens of seconds), the angular range scanned by the stepper motor cannot exceed several tens of arcseconds, and the number of scans using ABXO should not exceed 15–20. Possibly, the temporal resolution in a triple-crystal diffraction experiment can be increased by using two elements simultaneously instead of a combination of ABXO and step motor. Another way to increase temporal resolution is by using a linear detector instead of a point one.

3. Diffractometer

3.1. Experimental scheme

The principal scheme of the diffractometer TRS (Pinsker *et al.*, 1975) is shown in Fig. 2. This scheme was used for all triple-crystal diffraction experiments presented in this paper. In simpler double-crystal diffraction experiments, a point detector was mounted after the sample instead of the analyzer. The radiation source is an X-ray tube with a molybdenum anode.

The experimental scheme must be configured to diffraction conditions before applying an electric field to the ABXO element. In a double-crystal experiment, only the ABXO element is used for measurements after setting up the scheme.

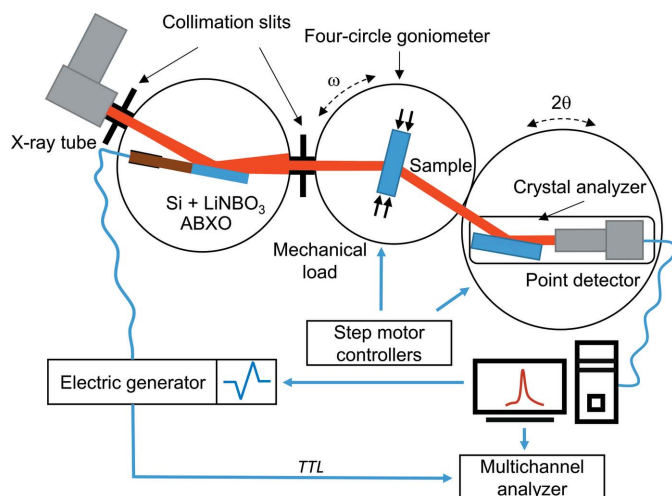


Figure 2

The principal experimental scheme includes an X-ray tube with a molybdenum anode; the ABXO element with an Si (110)-cut crystal as monochromator; collimating slits; a crystalline sample in transmission (as shown) or reflection geometry; an Si (110)-cut crystal analyzer; and a point scintillation detector.

In a triple-crystal experiment, both the ABXO element and the stepper motor of the ω or 2θ coordinate axis are used for data acquisition.

In the experimental scheme in Fig. 2, the ABXO element is installed as a monochromator. After ABXO element installation, all the capabilities of a conventional triple-axis diffractometer are retained. The ABXO can be installed on any conventional double-axis and triple-axis diffractometer.

For beam collimation, 0.15 mm slits were installed in front of and after the monochromator. Slits cut the peak tails, and only the characteristic Mo $K\alpha_1$ line passes.

A specialized holder for the ABXO element was designed, shown in Fig. 1(a). The element presented in this paper consists of two parts: a bimorph piezo actuator (bidomain LiNbO₃ single crystal with dimensions of 80 × 11 mm and a thickness of 1.0 mm) and a high-perfection silicon single-crystal plate with (110) surface orientation, dimensions of 35 × 25 mm and a thickness of 0.5 mm. Because of the ABXO element's high precision and sensibility (Kubasov *et al.*, 2019), it requires strong vibration protection.

In triple-crystal diffraction experiments, the point detector and the crystal analyzer are mounted on the same shoulder and moved simultaneously. Before measurements, the analyzer is set to the Bragg position and remains stationary relative to the detector during the registration of X-ray radiation.

In X-ray diffraction experiments the angular position of the ABXO element depends on the control signal phase. Thus, a data acquisition system based on a multichannel analyzer was developed. The multichannel analyzer records each X-ray pulse into channels depending on the registration time (oscillation phase of the ABXO element).

Calibration of the ABXO element is necessary before measurements. X-ray intensity versus channel number is recalculated to intensity versus angular seconds. Calibration is a procedure of comparison of rocking curves measured by the ABXO element with specified settings and classical double-crystal diffractometry (Eliovich *et al.*, 2018). The calibration algorithm is the same for RSMs because it is a set of sequentially recorded rocking curves.

For correct processing of diffraction data, it is necessary to consider the instrumental function of the diffractometer, which is a convolution of the angular and spectral distribution of radiation with the transmission functions of optical elements (Seregin *et al.*, 2019).

For time-resolved studies under uniaxial compression and vibration, specialized diffractometer modules have been designed.

3.2. Press for uniaxial compression

Mechanical stress has a significant effect on the properties of single crystals (Chidambaram *et al.*, 2006; Thompson *et al.*, 2006). For *in situ* X-ray diffraction experiments with compression, diamond anvil cells are widely used. However, they are mainly intended for the study of micrometre-sized samples (Jayaraman, 1983) at extremely high (hundreds of GPa) hydrostatic pressure. The sizes of crystals used in

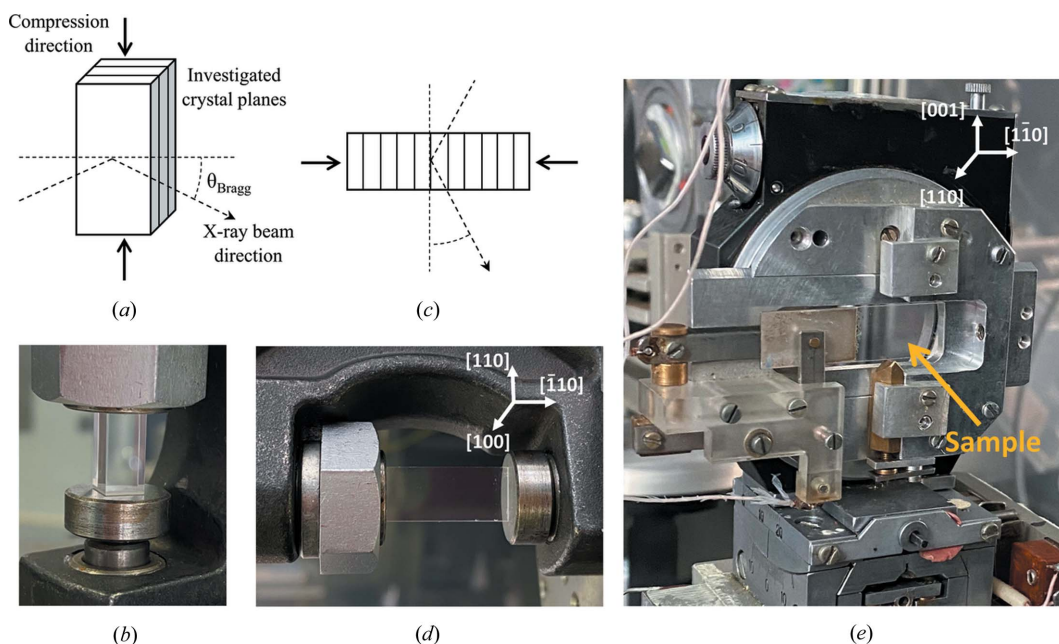


Figure 3 The experiment scheme in reflection geometry (a) and a photograph of the hydraulic press (b). The experiment scheme in transmission geometry (c) and a photograph of the hydraulic press (d). Photograph of the crystal holder for vibration load experiments (e) with an installed SiO₂ monolithic acoustic element. When an alternating electric field is applied to the SiO₂ element, the longitudinal vibrations occur in the [110] direction.

technology and industry are much larger, and a significant part of the deformation process occurs at lower loads.

A hydraulic press was developed specifically to study the effect of uniaxial mechanical load on single crystals. The press design (Fig. 3) allows one to create a uniaxial mechanical load of up to 5 tons on samples up to 30 × 20 × 20 mm in size. The maximum pressure (up to GPa) on the sample depends on the area of the loaded lateral faces. Thus, samples should have flat parallel lateral faces. The samples can be studied in transmission and reflection geometries. The load is measured by a strain gauge and transmitted to the controlling computer.

3.3. Vibration load system

Vibration load is a frequent phenomenon in technology, affecting the properties of semiconductor crystals from which electronic components are made (Steinberg, 2000; Uchida *et al.*, 2005). For example, in piezoelectric crystals, vibrations can cause electric fields. An effective method for generating a vibration load in a crystal is to excite an ultrasonic standing acoustic wave with MHz (Liss *et al.*, 1997; Zolotoyabko & Quintana, 2004) or kHz (Kovalchuk, 2011; Blagov *et al.*, 2013) frequency with an alternating electric field. This approach provides an opportunity to selectively excite crystal vibrations with large amplitude in a particular crystallographic direction. With X-ray diffraction, one can investigate the effect of these ultrasonic vibrations on the crystal planes. The possibility of investigating the properties of specific crystallographic directions in crystals of various syngonies under a controlled vibration load is of particular interest. However, this technique requires specialized sample preparation.

Single-crystal samples are prepared as composite or monolithic X-ray acoustic elements [Fig. 3(e)]. The composite

element consists of a sample crystal and a resonator crystal, which has a piezoelectric effect. Geometrical dimensions of crystals are selected so that both have the same natural vibration frequencies. If an electric field of this natural frequency is applied to the crystal resonator, it excites resonant longitudinal oscillations of the entire composite system (Blagov *et al.*, 2017). A monolithic X-ray acoustic element is a piezoelectric crystal, one half of which has a conductive coating and is a resonator, while the other half is the sample.

A specialized crystal holder is used for experiments with vibration load [Fig. 3(e)]. This holder provides X-ray diffraction measurements in Bragg and Laue geometry.

3.4. Control software

The diffractometer control, including the ABXO element, press and vibration load system, is carried out by an open-source TANGO environment (Fig. 4) (Chaize *et al.*, 1999). TANGO is used at synchrotron facilities, and its key

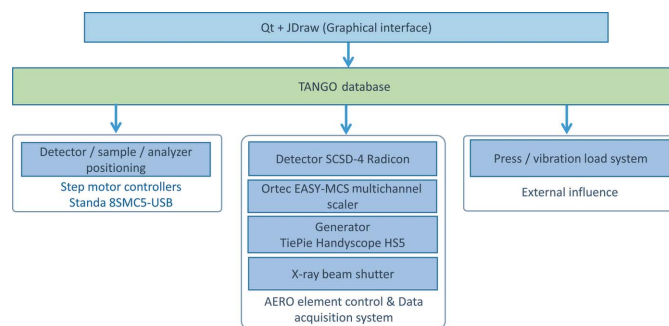
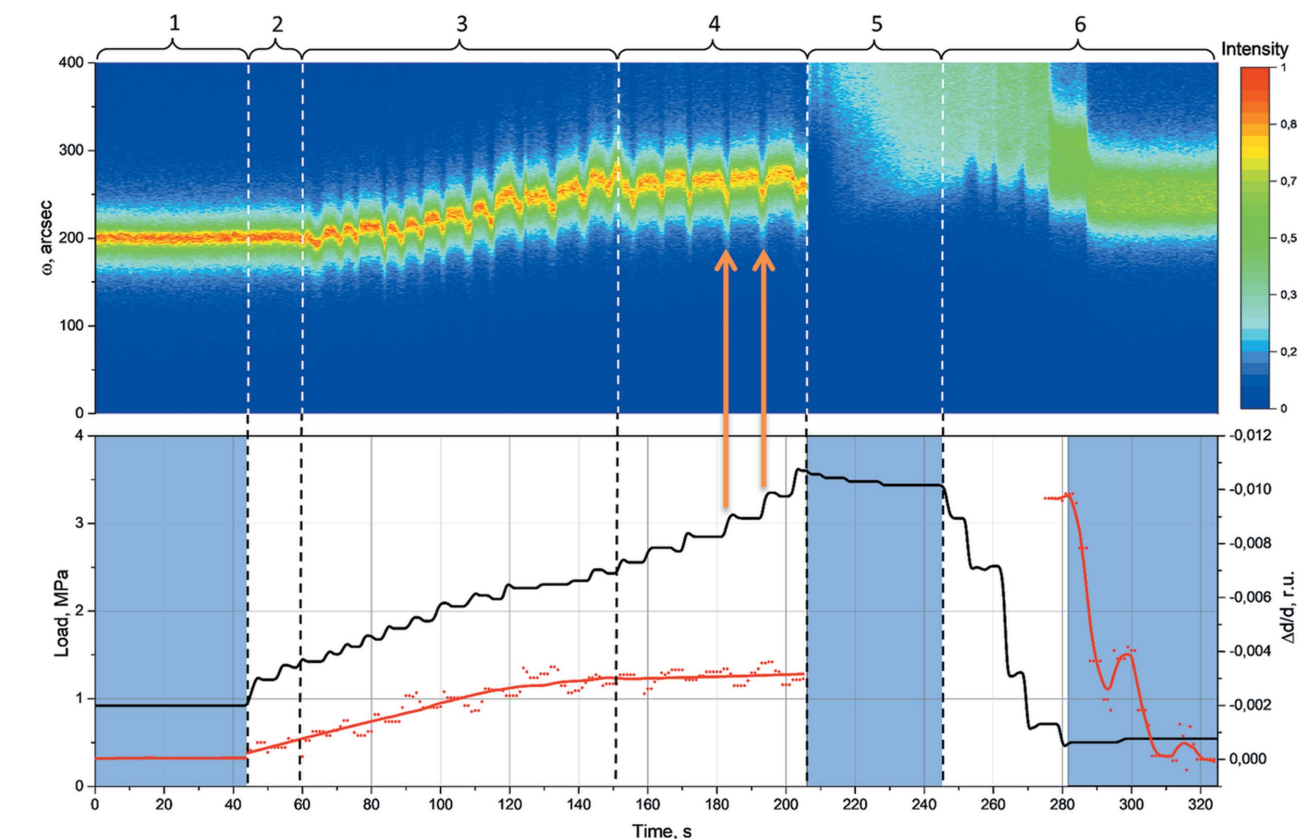
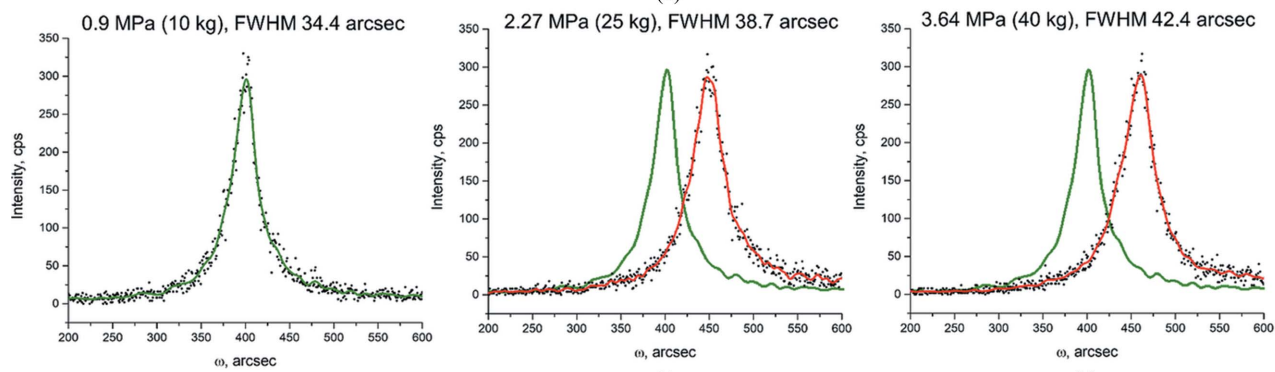


Figure 4 Scheme of the control software based on an open-source TANGO environment.



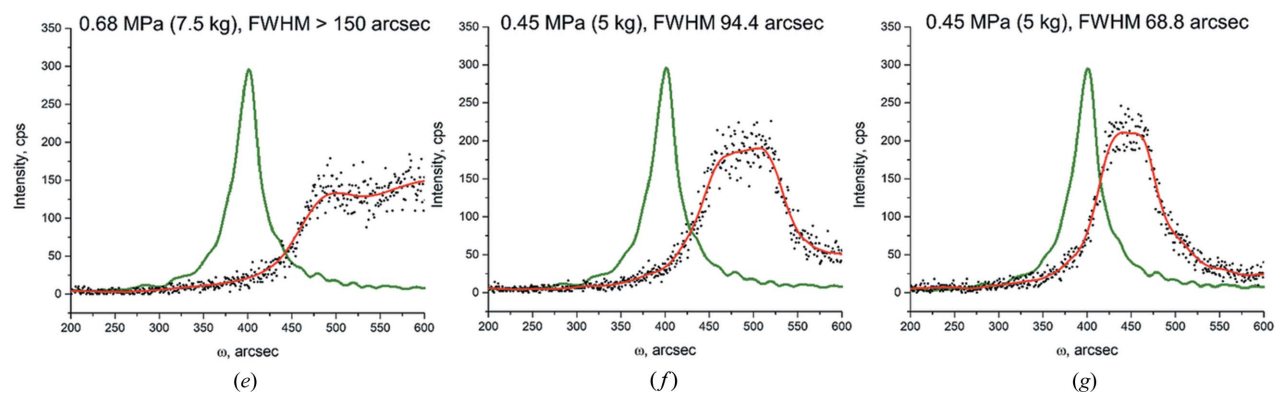
(a)



(b)

(c)

(d)



(e)

(f)

(g)

Figure 5

(a) A two-dimensional map of rocking curves versus time of the TeO_2 crystal under quasi-static load. The second part of the figure shows the load and relative strain $\Delta d/d$ versus time. Dotted lines indicate experiment stage boundaries described in Table 1. Blue areas indicate static load. Orange arrows indicate oscillations induced by press compression. (b) Double-crystal rocking curve measured by the ABXO element with 0.9 MPa load. Double-crystal rocking curves measured under uniaxial compression load of 2.27 (c), 3.64 (d), 0.68 (e), 0.45 (f) and 0.45 (g) MPa compared with (b).

Table 1
Load–unload cycle stages (RC = rocking curve).

Stage	Description	Start/final load (MPa)	RC parameters		
			Load (MPa)	FWHM (arcsec)	Peak maximum shift (arcsec)
1	RCs were registered with a static load of 10 kg.	0.91	0.91	34.4	0
2	The load increased, but the RC peak position and its shape did not change.	0.91/1.36	1.36	35.4	5.6
3	Uniform load increase induced a significant elastic deformation of the crystal. It caused peak FWHM increase and changed the angular position of the peak.	1.36/2.45	1.82	36.1	4.8
4	The angular position of the peak and the FWHM did not change with an increase in the load. The crystal deformation remained almost unchanged.	2.45/3.64	2.27	38.7	50.4
			2.45	41.6	64.4
			2.73	39.2	68.8
5	As a result of the deformation, the crystal structure quality abruptly changed. At this moment, the load increase was stopped, and the load remained constant for 40 s. The relaxation process inside the crystal affected the diffraction peak.	3.64/3.45	3.64	42.4	65.4
			3.45	>180	>225
			0.68	>150	158.5
6	The load gradually decreased. As a result, peak position and FWHM began to return to the initial values. The difference in RC parameters and position at the beginning and end of the load–unload cycle is caused by residual elastic deformation of the crystal planes.	3.45/0.45	0.45	94.4	85.6
			0.45	68.8	40.7
			0.45	68.8	40.7

advantage is the ability to manage different devices from a single software environment. A graphical interface was created using the *Qt* library and built-in *JDraw* interface development tool.

4. Results and discussion

The presented ABXO time-resolved technique is designed to study the deformation behavior of high-quality crystalline materials used in micro- and optoelectronics. The samples were chosen to demonstrate the possibilities of different ABXO operating modes for rocking curve measurement and reciprocal-space mapping with laboratory X-ray sources.

4.1. Time-resolved studies of paratellurite (TeO₂) single crystal under quasi-static uniaxial compression

A series of 415 double-crystal rocking curves were registered with a temporal resolution of 0.41 s with 0.41 s intervals. The ABXO element was operated in resonant mode with a 160 Hz control signal amplitude of 105 V. The sample was a TeO₂ single crystal, 16 × 10 × 11 mm in size. A face with (110) surface orientation was studied. All measurements were conducted in reflection geometry, in a quasi-dispersive (+*n*, −*m*) double-crystal scheme with 220 reflections from the silicon ($\theta_B = 10.644^\circ$) ABXO element and paratellurite ($\theta_B = 12.037^\circ$) sample.

Initially, the sample was set in a hydraulic press under a 0.91 MPa (10 kg) compression load applied along the [001] direction. The initial load is necessary for the fixation of the sample before measurements. In Fig. 5, one can observe the evolution of the shape and angular position of the rocking curves caused by uniaxial compression of the TeO₂ crystal. The process of loading and unloading lasted about 6 min. This process can be divided into six stages, as presented in Table 1. The load was increased and decreased in steps [Fig. 5(a)]. At the moments of increasing or decreasing the load on the sample (this process took several seconds), the diffraction peak oscillated. Comparing the two-dimensional map of the rocking curves and the dependence of mechanical load versus

time [Fig. 5(a)] shows that these oscillations (indicated by the orange arrows) occurred when the compression or decompression process was stopped.

4.2. Time-resolved studies of lithium fluoride (LiF) single crystal under vibration load

The effect of a short-term vibration load on a single crystal of lithium fluoride was investigated. A specialized diffractometer setup was used for applying vibration load, described previously.

In a double-crystal diffraction experiment, the ABXO element was installed as a monochromator and operated in a resonant mode. In resonant mode with a sinusoidal 160 Hz control signal with an amplitude of 105 V, the ABXO element scanned an angular range of about 650 arcsec. A 020 reflection ($\theta_B = 10.143^\circ$) of an LiF (100)-cut single-crystal sample was studied in transmission geometry in a quasi-dispersive (+*n*, −*m*) X-ray scheme with the 220 reflection of the silicon ($\theta_B = 10.644^\circ$) ABXO element. Temporal resolution for a single rocking curve was 9.58 s, with each curve consisting of 500 measurement points.

A contour map of the measured rocking curves is shown in Fig. 6(a). Rocking curves (RCs) 1–4 show the defect structure before exposure. An electric field with 130 kHz frequency and an amplitude of 75 V was applied to the sample after RC 4. RCs 5 and 6 show the beginning of structural changes under external stress. In RCs 7–12, the system comes into balance. After RC 12, the electric field was turned off, and RC 13 shows the system relaxation process to its initial state, which can be observed on RCs 14 and 15. Rocking curves measured before and after vibration load [Fig. 6(b)] coincide within the error limits except for the slight peak angular shift caused by external stress.

4.3. Reciprocal-space mapping of lithium fluoride (LiF) single crystal under uniaxial compression

Triple-crystal diffraction measurements of an LiF single crystal [Fig. 3(d)] under uniaxial compression were carried out. The ABXO element was installed as a monochromator

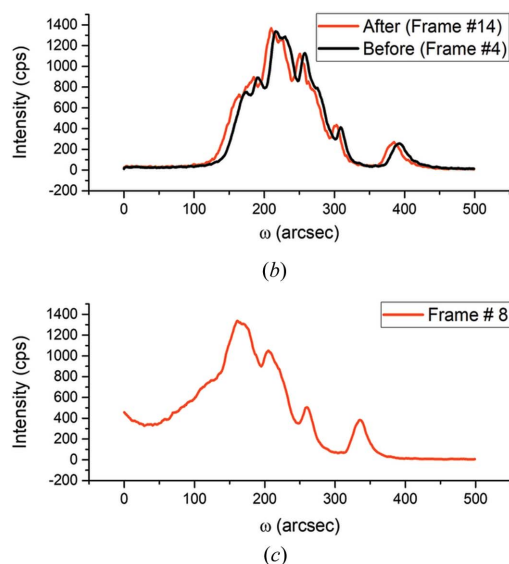
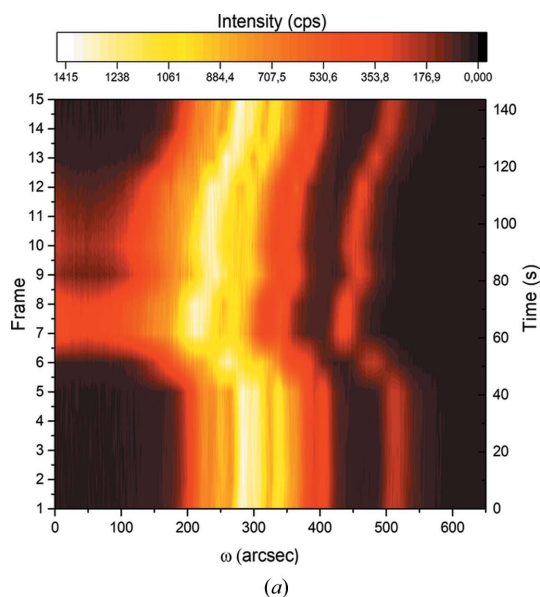


Figure 6
 (a) A two-dimensional map of rocking curves versus time. This map represents the defect structure evolution of the LiF single crystal under vibration load. (b) Rocking curves before and after vibration load. (c) A rocking curve of an LiF sample under vibration load.

and was used in resonant mode with a 160 Hz control signal amplitude of 105 V.

LiF single crystals are brittle, and have a low elastic limit (about 11.6 MPa) and good X-ray transparency. The sample crystal was a rectangular plate of $20 \times 10 \times 1$ mm. All measurements were conducted in transmission geometry, in a quasi-dispersive $(+n, -m, +n)$ scheme with 220 reflections from the silicon ($\theta_B = 10.644^\circ$) ABXO element and silicon analyzer and a 020 reflection ($\theta_B = 10.143^\circ$) from the (100)-cut lithium fluoride sample.

RSMs were collected for two cases: without load and under a uniaxial compression load of 6.5 kg (6.5 MPa). Each RSM was collected in about 1 h and is a two-dimensional matrix of 60 measurements (rocking curves). Every rocking curve has

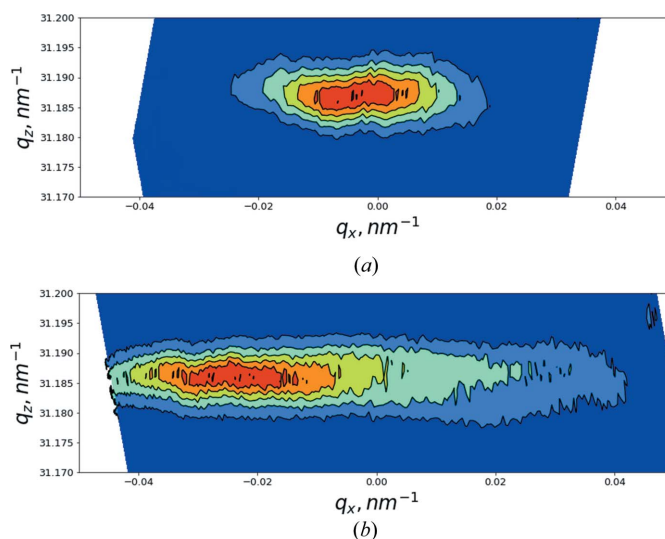


Figure 7
 (a) RSM of an LiF crystal without uniaxial compression load. (b) RSM of an LiF crystal under the uniaxial compression load of 6.5 MPa.

500 measurement points. This grid covers an area of about 700×300 arcsec in real space (along the β and 2θ axes).

A horizontal broadening of the diffraction spot was observed under compression [Fig. 7(b)]. This broadening indicates an increase in the disorientation of domains inside the crystal.

4.4. Reciprocal-space mapping of quartz (SiO_2) single crystal under vibration load

Triple-crystal diffraction measurements of an SiO_2 single crystal [Fig. 3(e)] were carried out. The ABXO element was installed as a monochromator and operated in resonant and quasi-static modes. In resonant mode, the 160 Hz control signal had an amplitude of 60 V [Figs. 8(a) and 8(c)]. In quasi-static mode, the 0.1 Hz control signal had an amplitude of 105 V [Fig. 8(b)]. The sample was a quartz monolithic acoustic element, 1 mm thick, with a natural frequency of 130 kHz.

All measurements were conducted in transmission geometry, in a quasi-dispersive $(+n, -m, +n)$ scheme with 220 reflections of the silicon ($\theta_B = 10.644^\circ$) ABXO element and silicon analyzer and the 220 reflection ($\theta_B = 9.5958^\circ$) of the (110)-cut quartz sample.

RSMs of the sample were acquired without vibration load [Fig. 8(a)] and under vibration load, controlled by an electric signal with 30 or 45 V amplitude [Figs. 8(b) and 8(c)]. Each RSM was acquired in about 35 min. In resonant mode, the collected data were a two-dimensional matrix of 71 scans, with 250 measurement points each, covering an area of 157.5×70 arcsec (along the β and 2θ axes). In the quasi-static mode case, the collected data were a two-dimensional matrix of 45 scans with 500 measurement points each, and covered an area of 46.2×44 arcsec.

Vibration load causes interplanar space (d) modulation with a natural frequency of 130 kHz. Modulation of interplanar space causes a significant broadening of the diffraction

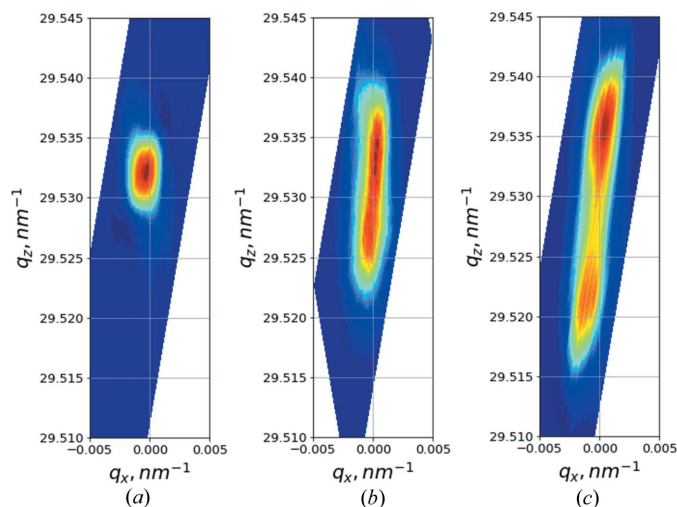


Figure 8 (a) RSM of a quartz crystal without vibrational load. (b), (c) RSMs of a quartz crystal under vibrational load induced by the electric field with different amplitudes: 30 V (b) and 45 V (c).

spot vertical size. With the increase of control signal amplitude, the interplanar space modulation increases. The diffraction spot inclination to the right, clearly visible in Figs. 8(b) and 8(c), is caused by a change in the X-ray diffraction angle upon interplanar space modulation.

5. Conclusions

A diffractometer with a single ABXO element can be used for time-resolved double-crystal diffraction experiments with subsecond temporal resolution and fast triple-crystal diffraction experiments (up to tens of seconds). The experimental scheme with a single ABXO element was tested for *in situ* measurements of reversible and irreversible processes in crystalline materials under uniaxial compression and vibration. For sample uniaxial quasi-static compression, a hydraulic press was designed with a load of up to 5 tons. A vibration load system was developed, including sample preparation and a crystal holder. The vibration load system allows control of the vibration power up to the value of sample destruction.

The presented diffractometer is a simple and powerful laboratory instrument for *in situ* studies of crystalline materials with traditional double-crystal and triple-crystal diffraction and an ABXO-based time-resolved technique.

Acknowledgements

The authors are grateful to the Department of Materials Science of Semiconductors and Dielectrics of NUST ‘MISIS’ for providing samples of the bidomain crystals.

Funding information

This work has been supported by the Russian Foundation for Basic Research, grant No. 19-29-12037 (to MK), and by the Ministry of Science and Higher Education of the Russian Federation, grant No. 075-15-2021-1362, as a part of the

development of X-ray techniques and in the framework of the work on the state assignment of the Federal Research Center for Crystallography and Photonics, Russian Academy of Sciences.

References

Blagov, A. E., Bykov, A. S., Kubasov, I. V., Malinkovich, M. D., Pisarevskii, Y. V., Targonskii, A. V., Eliovich, I. A. & Kovalchuk, M. V. (2016). *Instrum. Exp. Tech.* **59**, 728–732.

Blagov, A. E., Darinskii, A. N., Targonskii, A. V., Pisarevskii, Y. V., Prosekov, P. A. & Kovalchuk, M. V. (2013). *Acoust. Phys.* **59**, 506–512.

Blagov, A. E., Pisarevskii, Y. V., Targonskii, A. V., Eliovich, Y. A. & Kovalchuk, M. V. (2017). *Phys. Solid State*, **59**, 973–976.

Bowen, D. K. & Tanner, B. K. (1998). *High-Resolution X-ray Diffractometry and Topography*. London: Taylor and Francis.

Bukharaev, A. A., Zvezdin, A. K., Pyatakov, A. P. & Fetisov, Yu. K. (2018). *Phys.-Usp.* **61**, 1175–1212.

Bykov, A. S., Grigoryan, S. G., Zhukov, R. N., Kiselev, D. A., Ksenich, S. V., Kubasov, I. V., Malinkovich, M. D. & Parkhomenko, Y. N. (2014). *Russ. Microelectron.* **43**, 536–542.

Chaize, J.-M., Götz, A., Klotz, W.-D., Meyer, J., Pérez, M. & Taurel, E. (1999). *International Conference on Accelerator and Large Experimental Physics Control Systems, 1999, Trieste, Italy*, pp. 475–479.

Chidambaram, P. R., Bowen, C., Chakravarthi, S., Machala, C. & Wise, R. (2006). *IEEE Trans. Electron Devices*, **53**, 944–964.

Eliovich, I. A., Akkuratov, V. I., Targonskii, A. V. & Blagov, A. E. (2018). *Crystallogr. Rep.* **63**, 724–728.

Eliovich, I. A., Akkuratov, V. I., Targonskii, A. V., Prosekov, P. A., Blagov, A. E., Pisarevsky, Y. V. & Kovalchuk, M. V. (2020). *J. Synch. Investig.* **14**, 756–761.

Fewster, P. (1997). *Crit. Rev. Solid State Mater. Sci.* **22**, 69–110.

Filhol, F., Defaÿ, E., Divoux, C., Zinck, C. & Delaye, M.-T. (2005). *Sens. Actuators A Phys.* **123–124**, 483–489.

He, B. B. (2018). *Two-Dimensional X-ray Diffraction*. Hoboken: John Wiley & Sons.

Iida, A. & Kohra, K. (1979). *Phys. Status Solidi A*, **51**, 533–542.

Jayaraman, A. (1983). *Rev. Mod. Phys.* **55**, 65–108.

Kishimoto, S., Ishizawa, N. & Vaalsta, T. P. (1998). *Rev. Sci. Instrum.* **69**, 384–391.

Kohn, V. G., Kulikov, A. G., Prosekov, P. A., Seregin, A. Y., Targonsky, A. V., Eliovich, Y. A., Pisarevsky, Y. V., Blagov, A. E. & Kovalchuk, M. V. (2020). *J. Synchrotron Rad.* **27**, 378–385.

Kovalchuk, M. V. (2011). *Crystallogr. Rep.* **56**, 828–831.

Kubasov, I. V., Kislyuk, A. M., Turutin, A. V., Bykov, A. S., Kiselev, D. A., Temirov, A. A., Zhukov, R. N., Sobolev, N. A., Malinkovich, M. D. & Parkhomenko, Y. N. (2019). *Sensors*, **19**, 614.

Kulikov, A. G., Blagov, A. E., Marchenkov, N. V., Targonsky, A., Eliovich, Y., Pisarevsky, Y. & Kovalchuk, M. V. (2019). *Sens. Actuators A Phys.* **291**, 68–74.

Li, J., Shan, Z. & Ma, E. (2014). *MRS Bull.* **39**, 108–114.

Liss, K.-D., Magerl, A., Remhof, A. & Hock, R. (1997). *Acta Cryst.* **A53**, 181–186.

Malinkovich, M. D., Antipov, V. V. & Bykov, A. S. (2013). RF Patent 2492283.

Marchenkov, N. V., Kulikov, A. G., Targonsky, A. V., Eliovich, Y. A., Pisarevsky, Y. V., Seregin, A. Y., Blagov, A. E. & Kovalchuk, M. (2019). *Sens. Actuators A Phys.* **293**, 48–55.

Matsunami, G., Kawamata, A., Hosaka, H. & Morita, T. (2008). *Sens. Actuators A Phys.* **144**, 337–340.

Morita, T. (2003). *Sens. Actuators A Phys.* **103**, 291–300.

Nakamura, K. & Shimizu, H. (1989). *Ferroelectrics*, **93**, 211–216.

Nespolo, M. (2019). *J. Appl. Cryst.* **52**, 451–456.

Pietsch, U., Holy, V. & Baumbach, T. (2004). *High-Resolution X-ray Scattering: From Thin Films To Lateral Nanostructures*. New York: Springer Science & Business Media.

- Pinsker, Z. G., Kov'ev, E. K., Mirenskii, A. V., Fokin, A. S., Kovalchuk, M. V. & Shilin, Yu. A. (1975). USSR Inventor's Certificate No. 463045.
- Richwin, M., Zaeper, R., Lützenkirchen-Hecht, D. & Frahm, R. (2002). *Rev. Sci. Instrum.* **73**, 1668–1670.
- Seregin, A. Y., Prosekov, P. A., Chukhovskiy, F. N., Volkovsky, Y. A., Blagov, A. E. & Kovalchuk, M. V. (2019). *Crystallogr. Rep.* **64**, 545–552.
- Shur, V. Ya., Baturin, I. S., Mingaliev, E. A., Zorikhin, D. V., Udalov, A. R. & Greshnyakov, E. D. (2015). *Appl. Phys. Lett.* **106**, 053116.
- Sinno, T., Dornberger, E., von Ammon, W., Brown, R. A. & Dupret, F. (2000). *Mater. Sci. Eng. Rep.* **28**, 149–198.
- Steinberg, D. (2000). *Vibration Analysis for Electronic Equipment*. New York: John Wiley & Sons.
- Thompson, S. E., Sun, G., Choi, Y. S. & Nishida, T. (2006). *IEEE Trans. Electron Devices*, **53**, 1010–1020.
- Tsai, C. H., Tsai, C. W., Chang, H. T., Liu, S. H. & Tsai, J. C. (2015). *Sensors*, **15**, 14745–14756.
- Uchida, K., Krishnamohan, T., Saraswat, K. C. & Nishi, Y. (2005). *IEEE International Electron Devices Meeting, IEDM Technical Digest*, pp. 129–132. Washington, DC: IEEE.
- Zolotoyabko, E. & Quintana, J. P. (2004). *Rev. Sci. Instrum.* **75**, 699–708.